

A scalable optical detection scheme for matter wave interferometry

Alexander Stibor, André Stefanov, Fabienne Goldfarb¹,
Elisabeth Reiger, and Markus Arndt

Institut für Experimentalphysik, Universität Wien, Boltzmannngasse 5, A-1090 Wien

¹Laboratoire Aimé Cotton, F-91405 Orsay Cedex

E-mail: markus.arndt@univie.ac.at

Abstract. Imaging of surface adsorbed molecules is investigated as a novel detection method for matter wave interferometry with fluorescent particles. Mechanically magnified fluorescence imaging turns out to be an excellent tool for recording quantum interference patterns. It has a good sensitivity and yields patterns of high visibility. The spatial resolution of this technique is only determined by the Talbot gratings and can exceed the optical resolution limit by an order of magnitude. A unique advantage of this approach is its scalability: for certain classes of nanosized objects, the detection sensitivity will even increase significantly with increasing size of the particle.

PACS numbers: 03.65.Ta, 03.65.-w, 03.75.-b, 39.20.+q, 33.80.-b, 42.50.-p

1. Introduction

Recent years have seen a tremendous progress in the development of various matter wave interference experiments, using electrons [1, 2], large ultra-cold atomic ensembles [3], cold clusters [4, 5] or hot macromolecules [6, 7, 8]. Interferometry is also expected to lead to interesting applications in molecule metrology and molecule lithography. In particular quantum interference of complex systems is intriguing as it opens new ways for testing fundamental decoherence mechanisms [9].

Further progress along this line of research requires an efficient source, a versatile interferometer and a scalable detection scheme. Scalable sources represent still a significant technological challenge, but an appropriate interferometer scheme has already been suggested [10] and successfully implemented [7] for large molecules. All coherence experiments with clusters or molecules up to date finally employed ion detection. However, most ionization schemes run into efficiency limits when the mass and complexity of the particles increases [11]. Surface adsorption in combination with fluorescence detection is therefore a promising alternative. Its high efficiency will reduce the intensity constraints on future molecular beam sources for interferometry. It appears to be an important prerequisite not only for experiments exploring molecular coherence beyond 10,000 amu but also for decoherence and dephasing experiments with various dyes below 1,000 amu.

In the present article we demonstrate the feasibility of optically detecting matter wave interference fringes of dye molecules. Such structures usually have periods between 100...1000 nm and would be hardly resolved in direct imaging. But we show that a mechanical magnification step is a simple and very efficient technique to circumvent the optical resolution limit for interferograms. We can thus combine the high sensitivity of the fluorescence method with the high spatial resolution of our interferometer setup.

2. Experimental setup

2.1. Talbot-Lau interferometry with molecules

The idea behind the Talbot Lau interferometer has been previously described for instance in [12, 13, 7, 8] and the modification by our new detection scheme is shown in Fig. 1. Molecules, which pass the device, reveal their quantum wave nature by forming a regular density pattern at the location of the third grating. The distances between the gratings are equal in the experiment and corresponds to the Talbot length $L = 0.38$ m of molecules with a velocity of 250 m/s. It is chosen such that the period of the molecular fringe system is the same as that of the third grating. The regular interference pattern can then be visualized by recording the total transmitted molecular flux as a function of the position of the transversely scanning third grating.

The quantum wave nature of various large molecules was already studied in a similar interferometer but using either laser ionization [7] or electron impact ionization in combination with quadrupole mass spectrometry for the detection of the molecules [8].

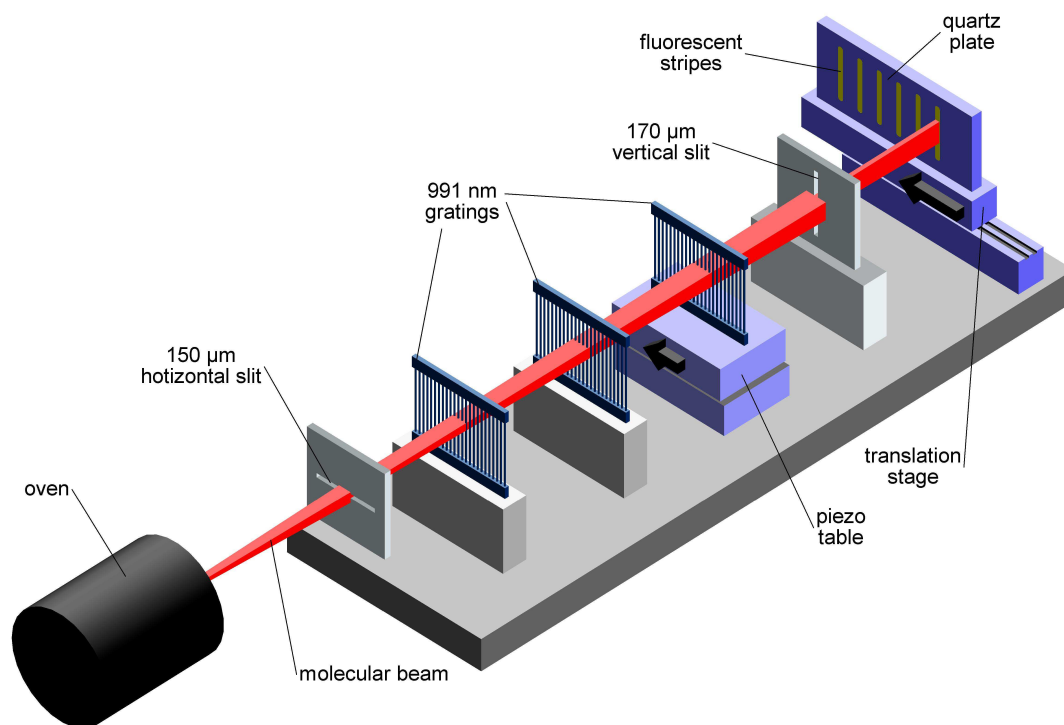


Figure 1. Mechanically magnified imaging of molecular interference patterns. All molecules passing the third grating are adsorbed on a plate which scans perpendicular to the molecular beam. The step-size of the adsorber is 4250 times larger than that of the third grating which is scanning along the same direction.

In spite of their success, both previous methods will probably be limited to masses below 10,000 amu. It is therefore important to develop a scalable detection scheme, such as fluorescence recording, which does not degrade but rather improve with molecular mass.

Molecule interferometry often operates with low particle numbers. Direct molecule counting in free flight therefore typically exhibits too weak signals [14]. In contrast to that, the light-exposure time of surface adsorbed molecules can exceed that of free-flying particles by orders of magnitude. When bound to a surface the molecules may also release part of their internal energy to the substrate. This helps in limiting the internal molecular temperature and in maximizing the number of fluorescent cycles. In our experiment the molecular beam was collected on a quartz plate behind the third grating. Several studies were done with similar aromatic molecules on silica or quartz surfaces. Due to their insulating properties the molecular fluorescence yield exceeds that on simple metals or semi-conductors [15].

2.2. Mechanically magnified fluorescence imaging

For demonstrating the feasibility of this novel detection method we chose meso-Tetraphenylporphyrin (TPP, Porphyrin Systems PO890001), a biodye with a mass of 614 amu. It exhibits sufficiently strong fluorescence, and a sufficiently high vapor pressure [14] to be evaporated in a thermal source which was set to a temperature of

about 420 °C. Moreover it was known to show quantum wave behavior in our setup [8]. Quadrupole mass spectroscopy allowed us to determine a mass purity of approximately 93%. A small contribution (7%) of porphyrin molecules lacked one phenyl ring. Smaller contaminations may contribute up to 2% to the mass in the initial powder but not to the fluorescence on the surface.

The adsorbing quartz surface was mounted on a motorized translation stage and it was shifted stepwise, parallel to the third grating as shown in Fig. 1. A fixed slit between the third grating and the quartz plate with a width of 170 μm limited the exposed area on the surface.

Molecules were deposited and accumulated over a time span of eight minutes under stationary conditions. Then the third grating, with a grating period of 991 nm, (about 400 nm open slits and a thickness of 500 nm) was shifted by 100 nm, and the adsorber plate was simultaneously displaced by 425 μm to an unexposed spot.

By repeating this process more than 30 times the third grating was moved over three periods and 30 stripes of fluorescent TPP molecules were accumulated on the surface. This way the molecular interference pattern was recorded with a mechanical magnification factor of 4250. The large (260 μm) gap between two stripes prevented any mixing of the molecules which could otherwise be caused by surface diffusion between the stripes. We have verified in independent diffusion experiments with TPP on quartz surfaces that the molecules aggregate and get immobilized on the 300...400 nm scale at room temperature.

With our new method the resolution is only limited by the dimensions of the gratings in the interferometer. These may have openings down to 50 nm and periods as small as 100 nm [16] as already used in earlier molecule interference experiments [6, 17].

2.3. Velocity selection

High contrast interferences fringes require that the molecular velocity spread be not too large. Actually for TPP and our present grating period of 990 nm a width of $\Delta v/v \simeq 10\%$ is sufficient. As in earlier experiments [7], this is done by selecting certain free-flight parabola of the molecules in the Earth's gravitational field using three horizontally oriented slits. The first slit is provided by the oven aperture of 200 μm , another slit of 150 μm width is placed 1.2 m away from the oven. The third point of the parabola is given by the vertical position on the detecting surface, which is located 2.9 m behind the oven. Fast molecules arrive at the top of the plate. Slow molecules, with a longer falling time, reach the surface at a lower position. In principle our method therefore provides the option to select the longitudinal coherence length a posteriori, after the experiment is already finished. However, in the present configuration the width of the velocity distribution is essentially determined by the size of the first two slits, since we integrate typically only over a much smaller position interval of 33 μm on the surface.

2.4. Surface preparation and fluorescence readout

An important requirement for the experiment is to have a perfectly clean substrate of low self-fluorescence. We used fused silica (suprasil I) of $500\text{ }\mu\text{m}$ thickness. It was cleaned from dust and organic solvents using the RCA-1 cleaning procedure [18] followed by methanol sonication and rinsing with ultrapure water. The clean surface was then bleached by an expanded 16 W argon ion laser beam for 30 minutes with an intensity of about 3 W/cm^2 . Owing to this preparation, no further bleaching could be observed and the background fluorescence was correspondingly low.

After depositing the molecules, the quartz plate was removed from the vacuum chamber and put under a fluorescence microscope (Zeiss; Axioskop 2 mot plus) in air, where a picture of each stripe was taken with an optical magnification factor of 20 and an integration time of 20 s. The irradiation intensity was 1.5 W/cm^2 . TPP absorbs well in the blue and emits in the red. Correspondingly, we used a standard mercury lamp (HBO 100) with an excitation filter transmitting wavelengths between 405 and 445 nm, a dichroic beam splitter with a pass band above 460 nm and an emission filter which transmitted above 600 nm.

At the chosen optical magnification and because of the limited size of the CCD camera (1 Megapixels) a single microscope image covers a height of $340\text{ }\mu\text{m}$. As the molecular beam is spread over about $3000\text{ }\mu\text{m}$ due to its velocity distribution, a whole picture matrix had to be recorded to image all velocity classes. Four rows of this 9×30 matrix selected around the positions with the highest molecular coverage are shown in Fig. 2.

The high quality of the data could be obtained because of the initial surface preparation and no smoothing was needed. The single images of one matrix row were arranged a bit closer to each other than they lie on the surface. Most of the empty gap between the stripes was removed for presentation purposes and their upper and lower ends were clipped to avoid regions of optical aberration.

From available vapor pressure data for porphyrins [14, 19], we estimate that around 0.1 monolayers of TPP reach the surface in eight minutes. Based on the work by [15] we assume that the fluorescence signal grows linearly with the deposition time within our experimental parameter range. Hence the fluorescence signal is proportional to the incident intensity, $I_i(x, y)$, the molecular fluorescence efficiency η , a geometrical collection factor $K(x, y)$ and to the molecular surface number density $N(x, y)$, which we want to determine:

$$I_f(x, y) = [\eta N(x, y) + B] \cdot K(x, y) I_i(x, y) + I_c(x, y) \quad (1)$$

where B is the background fluorescence emitted by the illuminated substrate and $I_c(x, y)$ represents the intrinsic detector noise. The surface sticking coefficient is assumed to be independent of the molecular surface coverage in our density regime and is included in N . The intensity of a reference image on a clean portion of the surface without molecules is

$$I_r(x, y) = BK(x, y)I_i(x, y) + I_c(x, y) \quad (2)$$

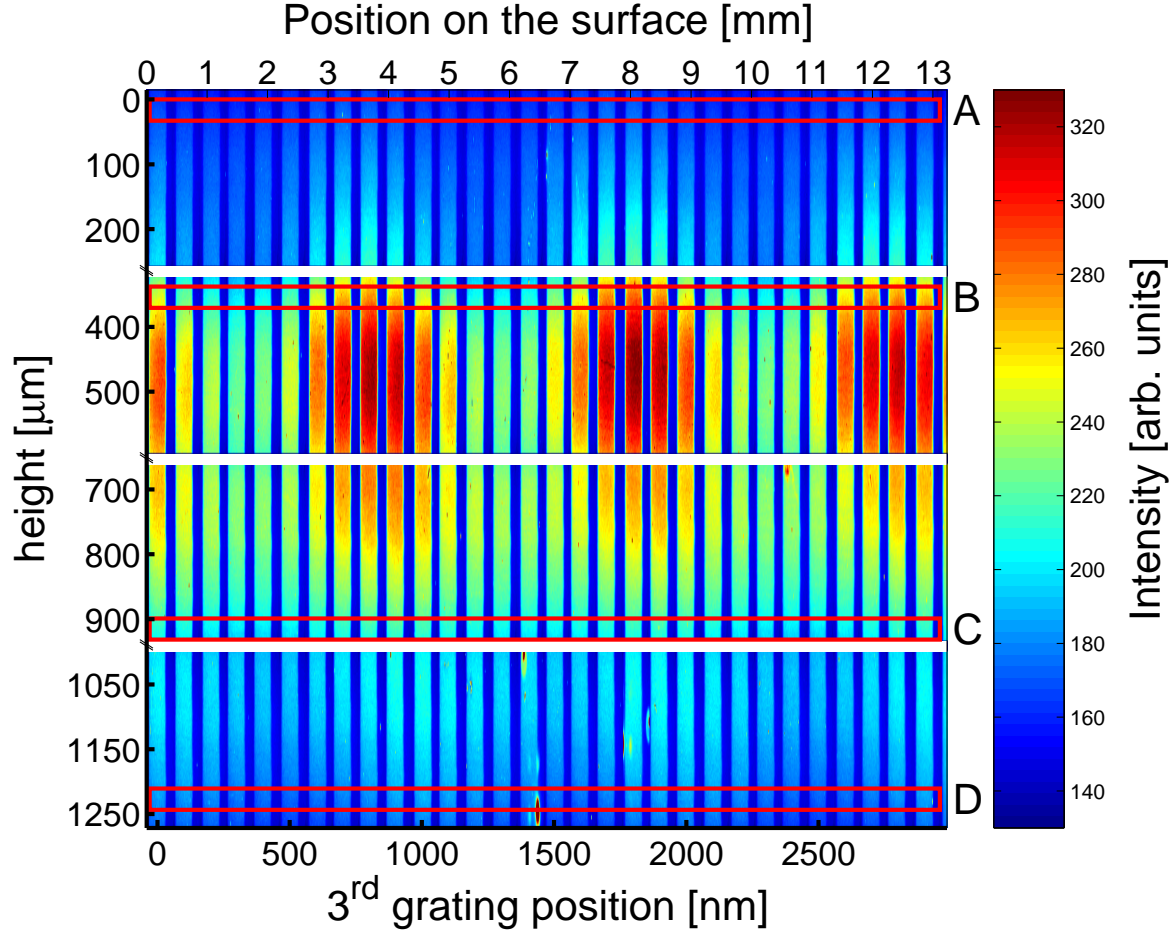


Figure 2. False color image of the measured fluorescent molecule density pattern on the surface. The images were corrected as described in the text. Each stripe corresponds to a given position of the third grating, and the vertical distribution encodes the molecular velocity. Four vertical cuts were made to measure the interference visibility of molecules with different velocities: A=33 μm ($v \approx 300$ m/s), B=371 μm ($v \approx 270$ m/s), C=938 μm ($v \approx 160$ m/s) and D=1234 μm ($v \approx 140$ m/s).

Using Eq. (1) and Eq. (2) we can evaluate from the experimental data the molecular surface density up to a constant factor

$$\tilde{N}(x, y) = \frac{\eta}{B} N(x, y) = \frac{I_f(x, y) - I_c(x, y)}{I_r(x, y) - I_c(x, y)} - 1$$

Fig. 2 shows the corrected intensity distribution $\tilde{N}(x, y)$. For each vertical stripe the total signal $\tilde{N}_{tot}(h)$ is computed by integrating $\tilde{N}(x, y)$ over a rectangle centered at position h in the middle of the stripe. The integration height is 33 μm and the width is 100 μm . The resulting intensity cross sections for four heights selected in Fig. 2 (A, B, C and D) are shown in Fig. 3. An evaluation of altogether 43 such interference curves allows to create a smooth plot of the interference fringe visibility versus the molecular velocity, as shown in Fig. 4. Note, that for TPP the velocity class with the highest contrast (b in Fig. 2 at $h=350$ μm) is very close but not equal to the most probable

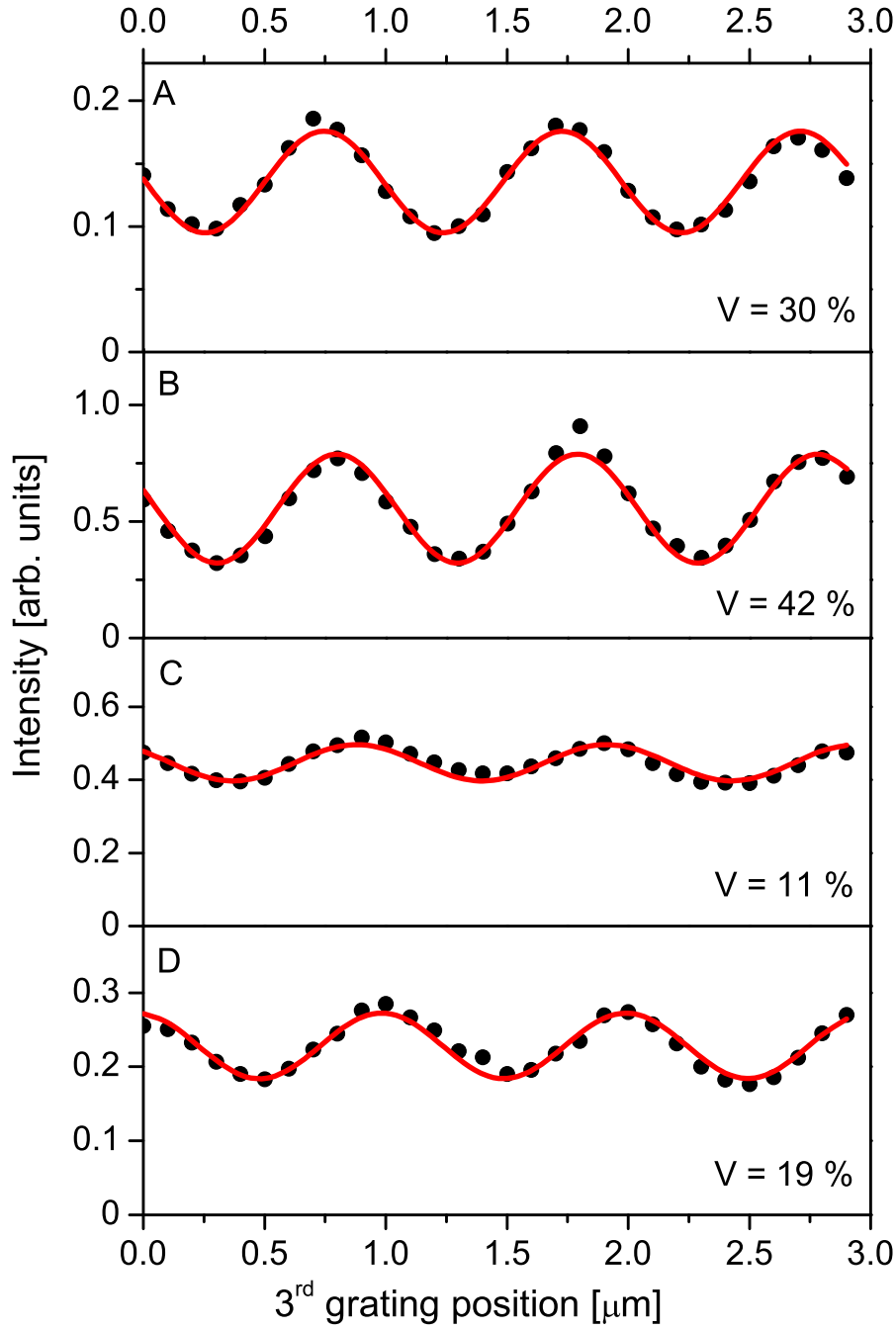


Figure 3. Interferences fringes extracted from the fluorescence images at different heights. The high contrast and its variation with velocity can only be explained by quantum interference. The labels A to D refer to Fig. 2.

velocity ($h=500 \mu\text{m}$).

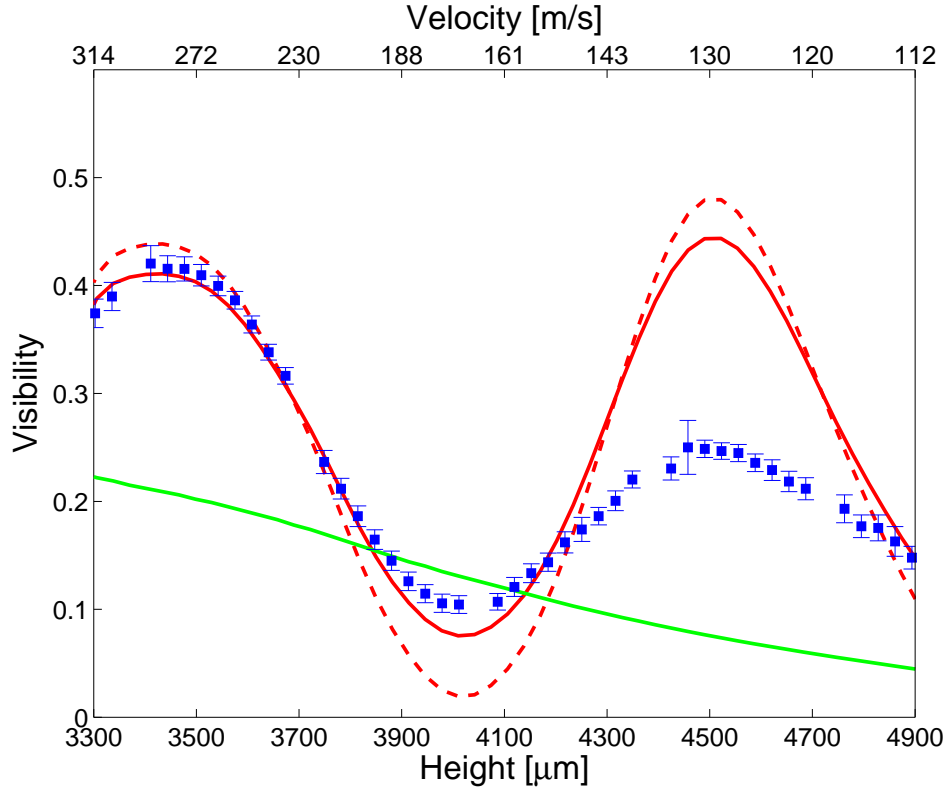


Figure 4. Visibility as a function of the deposition height. The dashed curve is computed by averaging over a velocity distribution whose mean is shown on the upper axis. The red plain curve is a corrected theory as described in the text. The green curve shows the contrast which would be expected by a classical Moiré effect. The experiment (full squares) clearly follows the quantum and not the classical model. Deviations at low velocities are discussed in the text.

3. Results

The experimental fringe visibility (full squares in Fig. 4) clearly varies in a non-monotonic and quasi-periodic way with the vertical molecular position on the detector, i.e. with the velocity or the de Broglie wavelength. The classical model, shown as the falling green line, cannot even qualitatively reproduce the velocity dependence of the fringe contrast – even if we take into account the van der Waals interaction with the grating walls as done here. The quantum prediction (dashed curve) also includes the molecule-grating interaction. It is computed by averaging the theoretical visibility over the velocity distribution, which is obtained from the geometry of our setup. The experimental contrast is well reproduced for fast molecules (about 250 m/s) and falls below the quantum model for velocities around 130 m/s. Slower molecules are more sensitive to both laboratory noise causing interferometer vibrations [20] and to collisional decoherence [21]. The observed contrast reduction for porphyrins at about 130 m/s is consistent with these effects. This is however not a fundamental limit, as in future experiments the present base pressure of 2×10^{-7} mbar in the interferometer chamber

can certainly be improved by about two orders of magnitude. And also mechanical vibrations should be suppressed by a factor of ten in future experiments with additional passive damping systems. The deviation at medium velocities is ascribed to molecules which do not follow a perfect free fall trajectory, because of scattering at edges along the beam path. In independent velocity measurements we have already observed before the effect of scattering, which deflects molecules of a given speed into the trajectory of another free-fall velocity class. The red continuous line shows the results of a model, which allows about 20% of the molecules at the most probable velocity to be spread out over the whole detector area. The resulting curve then fits indeed all experimental points, except those at low velocities, as discussed above.

Our accumulation and imaging method requires a good mechanical stability of the whole setup. From the good reproducibility of the expected and observed fringe period we derive an upper limit for the slow grating drift of 50 nm over four hours. A drift of 10 nm over this period is realistic in a second generation experiment.

A clear advantage of our new detection scheme is that all velocity classes are simultaneously recorded and encoded in the vertical position on the screen. This ensures utmost mechanical stability between the interferograms belonging to different velocities. The simultaneous recording can therefore be used to measure a possible phase shift between these interference fringes.

Ideally, we should not expect any velocity dependent phase shift in a symmetric Talbot Lau interferometer, where the distance between the first and second grating equals the distance between the second and the third one [23]. But an evaluation of Fig. 2 yields a phase variation in the vertical direction of about $0.4\pi/\text{mm}$ in our experiment. This effect can be traced back to a small angular misalignment between the gratings around the molecular beam axis. Our observation is for example consistent with a tilt as small as $200\ \mu\text{rad}$ between the second and the third grating.

The present detection scheme is therefore a very sensitive method for identifying the presence of such tilts, which will be important for interferometry with very massive molecules. Generally, the alignment requirements increase critically with increasing mass of the interfering particles [20].

In contrast to the present setup, other grating configurations may show additional non-classical effects, for instance the fractional Talbot effect [22]. In particular we do expect a phase jump of π between fringes of certain velocity classes [23] in an asymmetric Talbot Lau configuration. This is a non-classical feature which can still be observed in a regime where the classical Moiré effect and quantum interference are expected to yield comparable fringe visibilities. And the present experiment indicates that such features should be stably recorded using our new detection method, even in the presence of overall drifts of the interferometer.

4. Conclusion

Mechanically magnified fluorescence imaging offers several advantages for future experiments aiming at recording interferograms of nanometer-sized objects. The demonstrated method scales favorably with the complexity of the observed particles: organic molecules can be tagged with several dye molecules or semiconductor nanocrystals [24] and large proteins, such as GFP [25], or again nanocrystals [26] will even exhibit a much higher fluorescence quantum yield and a significantly smaller bleaching rate than the molecules in our current experiments. At present, the smallest commercially available fluorescent nanocrystals have a mass around 3000 amu [27][‡] in the core and roughly the same mass in the ligand shell. The high efficiency of our optical detection method will also allow to study the relevance of different electric and magnetic dipole moments in interference with molecules of rather similar masses, such as for example various porphyrin derivatives. Some of them have too low vapor pressures for experiments with ionization detectors, but will still be detectable in fluorescence. Mechanically magnified fluorescence imaging is therefore expected to be a scalable method for exploring the wave-particle duality of a large class of nanosized materials. It is an enabling technique for a range of dephasing and decoherence studies, which will also be useful in molecule metrology.

Acknowledgments

This work has been supported by the Austrian Science Fund (FWF), within the projects START Y177 and F1505 and by the European Commission under contract No. HPRN-CT-2002-00309 (QUACS). We acknowledge fruitful discussions with Klaus Hornberger, Lucia Hackermüller and Sarayut Deachapunya.

References

- [1] Freimund D L, Aflatooni K and Batelaan H 2001 *Nature* **413** 142
- [2] Ji Y, Chung Y, Sprinzak D, Heiblum M, Mahalu D and Shtrikman H 2003 *Nature* **422** 415
- [3] Andrews M R, Townsend C G, Miesner H J, Durfee D S, Kurn D M and Ketterle W 1997 *Science* **275** 637
- [4] Schöllkopf W and Toennies J P 1994 *Science* **266** 1345
- [5] Bruehl R, Guardiola R, Kalinin A, Kornilov O, Navarro J, Savas T and Toennies J P 2004 *Phys. Rev. Lett.* **92** 185301–1
- [6] Arndt M, Nairz O, Voss-Andreae J, Keller C, Van der Zouw G and Zeilinger A 1999 *Nature* **401** 680
- [7] Brezger B, Hackermüller L, Uttenthaler S, Petschinka J, Arndt M and Zeilinger A 2002 *Phys. Rev. Lett.* **88** 100404
- [8] Hackermüller L, Uttenthaler S, Hornberger K, Reiger E, Brezger B, Zeilinger A and Arndt M 2003 *Phys. Rev. Lett.* **91** 90408
- [9] Hackermüller L, Hornberger K, Brezger B, Zeilinger A and Arndt M 2004 *Nature* **427** 711

[‡] Evidenttech private communication: The masses of the quantum dots were recently measured by *Evidenttech* and turned out to be substantially smaller than found in earlier publications.

- [10] Clauser J F 1997 De Broglie-wave interference of small rocks and live viruses. Cohen R S, Horne M and Stachel J, editors, *Experimental Metaphysics* (Kluwer Academic)
- [11] Schlag E W, Grotemeyer J and Levine R D 1992 *Chem. Phys. Lett.* **190** 521
- [12] Clauser J F and Li S 1994 *Phys. Rev. A* **49** R2213
- [13] Dubetsky B and Berman P R 1997 Atom interference using microfabricated structures. Berman P R, editor, San Diego *Atom Interferometry* (Academic Press) 407-468,
- [14] Stefanov A, Stibor A, Dominguez-Clarimon A and Arndt M 2004 *J. Chem. Phys.* **121** 6935
- [15] Tanimura K, Kawai T and Sakata T 1980 *J. Phys. Chem.* **84** 751
- [16] Savas T A, Shah S N, Schattenburg M L, Carter J M and Smith H I 1995 *J. Vac. Sci. Technol. B* **13** 2732
- [17] Brühl R, Fouquet P, Grisenti R E, Toennies J P, Hegerfeldt G C, Köhler T, M Stoll and Walter C 2002 *Europhys. Lett.* **59** 357
- [18] Kern W and Puotinen D A 1970 *RCA Rev.* **31** 187
- [19] Perlovich G L, Golubchikov O A and Klueva M E 2000 *Journal of Porphyrins and Phthalocyanines* **4** 699
- [20] Stibor A, Hornberger K, Hackermüller L, Zeilinger A and Arndt M 2005 *Laser Physics* **15** 10
- [21] Hornberger K, Uttenthaler S, Brezger B, Hackermüller L, Arndt M and Zeilinger A 2003 *Phys. Rev. Lett.* **90** 160401
- [22] Berry M, Marzoli I, Schleich W, June 2001 *Physics World* 39
- [23] Brezger B, Arndt M and Zeilinger A 2003 *J. Opt. B: Quantum Semiclass. Opt.* **5** 82
- [24] Bruchez M Jr, Moronne M, Gin P, Weiss S and Alivisatos A P 1998 *Science* **281** 2013
- [25] Chalfie M and Kain S 1998 *Green Fluorescent Protein: Properties, Applications, and Protocols*. New York (Wiley-Liss)
- [26] Alivisatos A P 1996 *Science* **271** 933
- [27] <http://www.evidenttech.com/>